

# LHC discovery potential of the lightest NMSSM Higgs in the $h_1 \rightarrow a_1 a_1 \rightarrow 4\mu$ channel

Alexander Belyaev,<sup>1,2</sup> Jim Pivarski,<sup>3</sup> Alexei Safonov,<sup>3</sup> Sergey Senkin,<sup>3</sup> and Aysen Tatarinov<sup>3</sup>

<sup>1</sup> *School of Physics & Astronomy, University of Southampton,  
Highfield, Southampton SO17 1BJ, UK*

<sup>2</sup> *Particle Physics Department, Rutherford Appleton Laboratory,  
Chilton, Didcot, Oxon OX11 0QX, UK*

<sup>3</sup> *Department of Physics and Astronomy, Texas A&M University,  
College Station, TX 77843, USA*

(Dated: November 26, 2024)

We explore the potential of the Large Hadron Collider to observe the  $h_1 \rightarrow a_1 a_1 \rightarrow 4\mu$  signal from the lightest scalar Higgs boson ( $h_1$ ) decaying into the two lightest pseudoscalar Higgs bosons ( $a_1$ ), followed by their decays into four muons in the Next-to-Minimal Supersymmetric Standard Model (NMSSM). The signature under study applies to the region of the NMSSM parameter space in which  $m_{a_1} < 2m_\tau$ , which has not been studied previously. In such a scenario, the suggested strategy of searching for a four-muon signal with the appropriate background suppression would provide a powerful method to discover the lightest CP-even and CP-odd NMSSM Higgs bosons  $h_1$  and  $a_1$ .

## INTRODUCTION

The Next-to-Minimal Supersymmetric Standard Model (NMSSM) [1–13] extends the particle content of the Minimal Supersymmetric Standard Model (MSSM) by one singlet superfield. The NMSSM has several attractive features beyond the MSSM. First, the NMSSM elegantly solves the so-called  $\mu$  problem [14]: the scale of the  $\mu$  parameter is dynamically generated at the electroweak or SUSY scale when the singlet Higgs acquires a Vacuum Expectation Value (VEV). Second, the fine-tuning and little hierarchy problems of the NMSSM are greatly diminished compared to the MSSM [15]. In the NMSSM, the upper mass limit on the lightest CP-even Higgs boson is higher than in the MSSM, making it less constrained experimentally. Another attractive feature of the NMSSM is that the lightest CP-even Higgs can have a significant branching fraction for the new  $h_1 \rightarrow a_1 a_1$  decay ( $h_1$  and  $a_1$  are the lightest CP-even and CP-odd Higgs bosons, respectively). This weakens the LEP-II constraints on the allowed Higgs parameter space, as this new decay channel reduces the branching fractions of  $h_1$  into the modes used in direct Higgs searches. In addition, there are interesting implications in the cosmological Dark Matter sector of the model due to the appearance of the fifth neutralino, the “singlino.” It has been shown [16] that the NMSSM is consistent with the experimentally measured relic density, and the data provide important constraints on the allowed NMSSM parameters.

The rich phenomenology offered by the NMSSM, stemming from the extension of the scalar sector, has been the focus of numerous studies [17–25]. In Ref. [18], the first attempt to establish a “no-lose” theorem for NMSSM was presented. This theorem states that the Large Hadron Collider (LHC) has the potential to discover at least one NMSSM Higgs boson in the conventional mode, assuming that Higgs-to-Higgs decay modes are not important.

However, the fact that Higgs-to-Higgs decay modes can be important has been shown in analyses devoted to re-establishing the ‘no-lose’ theorem [19–25] in the case where the  $h_1 \rightarrow a_1 a_1$  branching fractions are significant and  $a_1$  is light. NMSSM scenarios with  $m_{a_1}$  between the  $2\tau$  and  $2b$ -quark thresholds ( $2m_\tau < m_{a_1} < 2m_b$ ) have previously been considered, focusing on the  $4\tau$  [25] channels in Higgs-strahlung and Vector Boson Fusion, establishing the NMSSM No-Lose Theorem at the LHC [25] for this  $a_1$  mass region. Future analysis of the  $4\tau$  channel is likely to be technically challenging and can only be performed with large datasets (typical integrated luminosity of 10–100 fb<sup>−1</sup>). A more recent study [26] has focused on the same region using the  $h_1 \rightarrow a_1 a_1 \rightarrow 2\mu 2\tau$  process, which has the benefit that the invariant mass of two muons forms a much narrower peak, improving the sensitivity of such an analysis in spite of the large reduction in signal yield due to small  $\mathcal{B}(a_1 \rightarrow \mu\mu)$ . Our findings indicate a substantially higher QCD multi-jet background contamination as compared to Ref. [26], which may have a substantial effect of the sensitivity of such a search.

In this paper, we explore the region in which the  $a_1$  mass is below the  $2\tau$  threshold ( $m_{a_1} < 2m_\tau$ ). For this case, which has not been studied previously, we explore the potential of the  $h_1 \rightarrow a_1 a_1 \rightarrow 4\mu$  signature at the LHC. Unlike searches for the  $4\tau$  signature, the invariant mass of each muon pair provides a direct estimate of  $m_{a_1}$  and the  $4\mu$  invariant mass provides  $m_{h_1}$ . Use of these kinematic constraints leads to essentially zero background and therefore allows one to rely on direct  $gg$  and  $b\bar{b}$  fusion for Higgs production instead of the subdominant vector boson fusion or associated production processes chosen in the  $4\tau$  search [18] to suppress QCD backgrounds.

We demonstrate that the analysis of the  $4\mu$  mode has excellent sensitivity to  $h_1$  production, can be performed with early LHC data, and requires little in terms of detector performance except reasonably robust muon tracking and identification. To present a realistic analysis, we

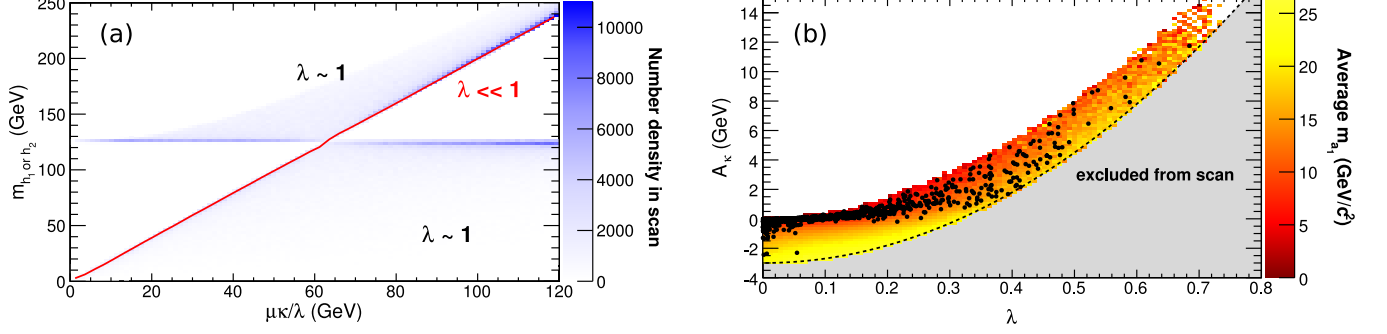


FIG. 1: (a): Mass of the lightest (\$h\_1\$) and second-lightest (\$h\_2\$) CP-even Higgses as a function of \$\mu\kappa/\lambda\$ and \$\lambda\$. The density of generated scenarios surviving constraints is shown in the blue color scale, and the red line represents the single-valued \$\lambda \ll 1\$ limit (mean of \$\lambda < 0.01\$ scenarios). (b): Mass of the lightest CP-odd Higgs (\$a\_1\$) as a function of \$A\_\kappa\$ and \$\lambda\$. The color scale is the average mass in each bin, and filled circles are the scenarios with \$m\_{a\_1} < 2m\_\tau\$. The edge of the low \$m\_{a\_1}\$ region follows a parabolic curve, \$(30 \text{ GeV})\lambda^2 - A\_\kappa \simeq 0\$.

use parameters of the CMS detector at the LHC to design event selection and to estimate background contributions.

The rest of the paper is organized as follows. In Section II, we study the NMSSM parameter space in which \$m\_{a\_1} < 2m\_\tau\$ and discuss the phenomenology of the model. In Section III, we review constraints on the NMSSM parameter space from existing data. In Section IV, we outline the proposed analysis for the \$4\mu\$ mode and evaluate its sensitivity. Final conclusions are presented in Section V.

### NMSSM PARAMETER SPACE

In our study we consider the simplest version of the NMSSM [1–12], in which the \$\mu\widehat{H}\_1\widehat{H}\_2\$ term of the MSSM superpotential is replaced by

$$\lambda\widehat{S}\widehat{H}_1\widehat{H}_2 + \frac{\kappa}{3}\widehat{S}^3, \quad (1)$$

making the superpotential scale-invariant. In general, there are five soft breaking terms; in the “non-universal” case,

$$m_{H_1}^2 H_1^2 + m_{H_2}^2 H_2^2 + m_S^2 S^2 + \lambda A_\lambda H_1 H_2 S + \frac{\kappa}{3} A_\kappa S^3. \quad (2)$$

In the above equations, capital letters with tildes denote superfields while symbols without tildes denote the scalar component of the respective superfield.

Soft breaking parameters in Eq.(2), \$m\_{H\_1}^2\$, \$m\_{H\_2}^2\$ and \$m\_S^2\$, can be expressed in terms of \$M\_Z\$, the ratio of the doublet Higgs VEVs, \$\tan\beta\$, and \$\mu = \lambda s\$ (where \$s = \langle S \rangle\$, the VEV of the singlet Higgs field) through the three minimization equations of the Higgs potential. Assuming that the Higgs sector is CP-conserving, the NMSSM Higgs sector at the Electro-Weak (EW) scale is uniquely defined by 14 parameters: \$\tan\beta\$, the trilinear couplings in

the superpotential, \$\lambda\$ and \$\kappa\$, the corresponding soft SUSY breaking parameters \$A\_\lambda\$ and \$A\_\kappa\$, the effective \$\mu\$ parameter \$\mu = \lambda s\$, the gaugino mass parameters \$M\_1\$, \$M\_2\$, and \$M\_3\$, the squark and slepton trilinear couplings \$A\_t\$, \$A\_b\$, and \$A\_\tau\$, and the squark and slepton mass parameters \$M\_{f\_L}\$ and \$M\_{f\_R}\$. For simplicity, we assume universality within 3 generations for the last two parameters, leaving only 6 parameters for sfermion masses.

### Parameter Scan of the Low-\$m\_{a\_1}\$ Region of the NMSSM

To find the parameter space for our region of interest, \$m\_{a\_1} < 2m\_\tau\$, we scan the NMSSM parameters using the NMSSMTools package [27–29], applying all known phenomenological and experimental constraints except the following: the cosmological dark matter relic density measured by WMAP [30], the direct \$p\bar{p} \rightarrow h\_1 \rightarrow a\_1 a\_1 \rightarrow 4\mu\$ search by the Tevatron [31], the direct \$e^+e^- \rightarrow Zh\_1\$, \$h\_1 \rightarrow a\_1 a\_1\$ searches by LEP [32, 33], the direct \$\Upsilon \rightarrow \gamma a\_1\$ searches by CLEO [34] and BaBar [35], and limits set by rare \$B \rightarrow K \ell^+ \ell^-\$ decays [36]. These important constraints are explicitly studied in our region of interest in a later section.

In our scan, we fix parameters entering the Higgs sector at loop-level to \$M\_1/M\_2/M\_3 = 150/300/1000\$ GeV, \$A\_t = A\_b = A\_\tau = 2.5\$ TeV, and \$M\_{f\_L} = M\_{f\_R} = 1\$ TeV. We then sample the NMSSM model points uniformly in a six-dimensional space. The first four scan parameters are conventional, broad ranges over the probable values of \$\mu\$, \$\lambda\$, \$\tan\beta\$, and \$A\_\lambda\$:

- \$100 \text{ GeV} < \mu < 1000 \text{ GeV}\$
- \$0 < \lambda < 1\$
- \$1.5 < \tan\beta < 50\$

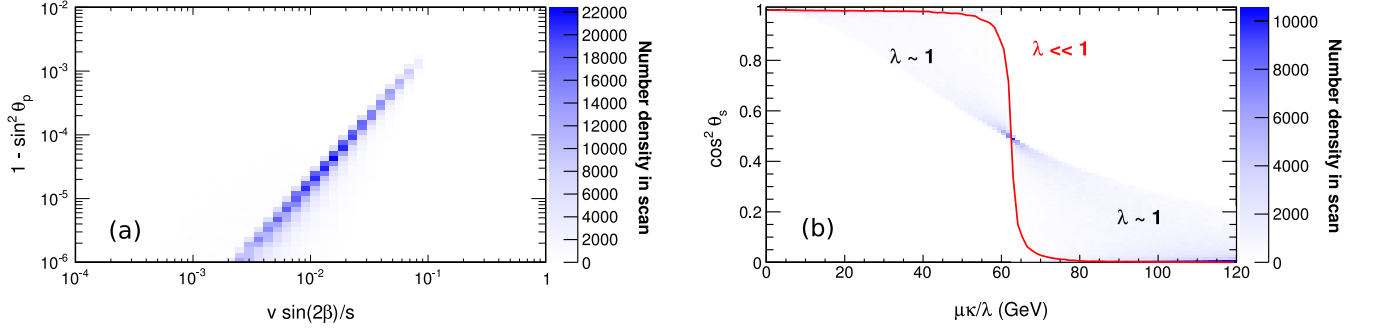


FIG. 2: (a): Non-singlet fraction  $1 - \sin^2 \theta_P$  of the lightest CP-odd Higgs boson ( $a_1$ ) as a function of  $v \sin 2\beta/s$ . (b): Singlet fraction  $\cos^2 \theta_S$  of the lightest CP-even Higgs boson ( $h_1$ ) as a function of  $\mu\kappa/\lambda$ . (The red line is the mean of  $\lambda < 0.01$  scenarios.)

- $-1 \text{ TeV} < A_\lambda < 5 \text{ TeV}$

For the two remaining parameters, we identify two additional phenomenological variables that allow a more narrow selection of the region of interest and simplify the interpretation of our observations. A theoretical justification of these variables is discussed in the next section. The first of these two parameters,  $\mu\kappa/\lambda = \kappa s$ , is selected because of its correlation with the mass of the CP-even Higgs bosons, see Fig. 1(a). The corresponding range used in the scan

- $0 < \mu\kappa/\lambda < 120 \text{ GeV}$

was chosen to include two equally sized but phenomenologically different sub-domains; in the lower one  $h_1$  is light and  $h_2$  is the SM-like Higgs, and in the upper one  $h_1$  is the SM-like Higgs.

The final parameter and its scan range,

- $0 \text{ GeV} < (30 \text{ GeV})\lambda^2 - A_\kappa < 3 \text{ GeV}$ ,

are chosen to zoom into the region of low  $a_1$  masses as illustrated in Fig. 1(b).

### Higgs Sector Spectrum and Mixings

The CP-even and CP-odd Higgs mass matrices,  $\mathcal{M}_S$  and  $\mathcal{M}_P$ , can be written as [27]:

$$\begin{aligned}
 \mathcal{M}_{S11}^2 &= g^2 v^2 \sin^2 \beta^2 + \mu \tan \beta (A_\lambda + \kappa s) \\
 \mathcal{M}_{S22}^2 &= g^2 v^2 \cos^2 \beta^2 + \mu \cot \beta (A_\lambda + \kappa s) \\
 \mathcal{M}_{S33}^2 &= \lambda A_\lambda \frac{v^2 \sin 2\beta}{2s} + \kappa s (A_\kappa + 4\kappa s) \\
 \mathcal{M}_{S12}^2 &= (\lambda^2 - g^2/2) v^2 \sin 2\beta - \lambda s (A_\lambda + \kappa s) \\
 \mathcal{M}_{S13}^2 &= \lambda v (2\lambda s \cos \beta - \sin \beta (A_\lambda + 2\kappa s)) \\
 \mathcal{M}_{S23}^2 &= \lambda v (2\lambda s \sin \beta - \cos \beta (A_\lambda + 2\kappa s)) \quad (3)
 \end{aligned}$$

$$\begin{aligned}
 \mathcal{M}_{P11}^2 &= \frac{2\lambda s}{\sin 2\beta} (A_\lambda + \kappa s) \\
 \mathcal{M}_{P22}^2 &= 2\lambda \kappa v^2 \sin 2\beta + \lambda A_\lambda \frac{v^2 \sin 2\beta}{2s} - 3\kappa A_\kappa s \\
 \mathcal{M}_{P12}^2 &= \lambda v (A_\lambda - 2\kappa s) \quad (4)
 \end{aligned}$$

In general,  $a_1$  is light in the regions of the parameter space approaching either the Peccei-Quinn (PQ) symmetry limit ( $\kappa \rightarrow 0$ ) or the R-symmetry (RS) limit ( $A_\kappa, A_\lambda \rightarrow 0$ ). In both limits,  $a_1$  is a massless axion, a fact which directly follows from Eq.(4). It can be decomposed in terms of the weak eigenstates  $H_{uI}$ ,  $H_{dI}$ , and  $S_I$  as (see e.g.[37]):

$$a_1 = \cos \theta_P A + \sin \theta_P S_I, \quad (5)$$

where  $A = \cos \beta H_{uI} + \sin \beta H_{dI}$ . In the PQ limit, the mixing parameters  $\cos \theta_P$  and  $\sin \theta_P$  are

$$\cos \theta_P = \frac{v \sin 2\beta}{\sqrt{v^2 \sin^2 2\beta + 4s^2}}, \sin \theta_P = -\frac{2s}{\sqrt{v^2 \sin^2 2\beta + 4s^2}}. \quad (6)$$

In the RS limit, the same parameters are

$$\cos \theta_P = \frac{v \sin 2\beta}{\sqrt{v^2 \sin^2 2\beta + s^2}}, \sin \theta_P = \frac{s}{\sqrt{v^2 \sin^2 2\beta + s^2}}. \quad (7)$$

According to Eq.(6,7), the non-singlet component of  $a_1$  is determined by the ratio  $v \sin 2\beta/s$ . Figure 2(a) shows evident correlation of the non-singlet fraction  $1 - \sin^2 \theta_P$  of the lightest pseudoscalar Higgs boson  $a_1$  with  $v \sin 2\beta/s$ , corresponding primarily to the PQ limit, as can be deduced from the slope of the correlation. It also demonstrates that in the region of interest  $a_1$  is nearly a pure singlet,  $1 - \sin^2 \theta_P^2 < 1\%$ , and that the values of  $v \sin 2\beta/s$  are always below 0.1. If we define  $\epsilon = v \sin 2\beta/s$ , then up to  $\mathcal{O}(\epsilon)$ ,  $\mathcal{O}(\kappa^2)$ , and  $\mathcal{O}(\lambda^2)$ , the

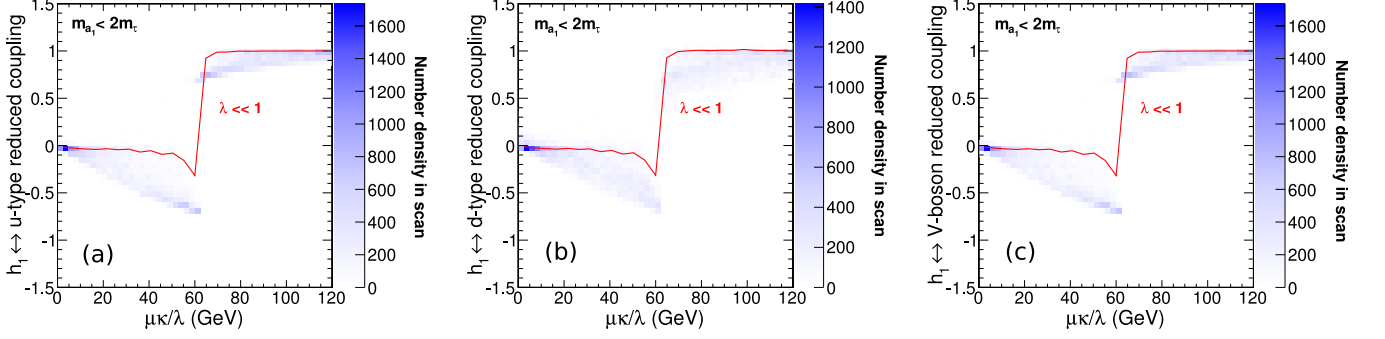


FIG. 3: Reduced couplings of  $h_1$  to up-type quarks (a), down-type quarks (b), and vector bosons (c) as a function of  $\mu\kappa/\lambda$ , with the requirement that  $m_{a_1} < 2m_\tau$ . (The red line is a mean of  $\lambda < 0.01$  scenarios.)

CP-even Higgs mass matrix can be re-written as

$$M_S^2 = \lambda s \quad (8)$$

$$\begin{pmatrix} (A_\lambda + s\kappa) \tan \beta & -(A_\lambda + s\kappa) & \epsilon \left( \frac{\lambda s}{\sin \beta} - \frac{A_\lambda + 2s\kappa}{2 \cos \beta} \right) \\ -(A_\lambda + s\kappa) & (A_\lambda + s\kappa) \cot \beta & \epsilon \left( \frac{\lambda s}{\cos \beta} - \frac{A_\lambda + 2s\kappa}{2 \sin \beta} \right) \\ \epsilon \left( \frac{\lambda s}{\sin \beta} - \frac{A_\lambda + 2s\kappa}{2 \cos \beta} \right) & \epsilon \left( \frac{\lambda s}{\cos \beta} - \frac{A_\lambda + 2s\kappa}{2 \sin \beta} \right) & \kappa \frac{A_\kappa + 4s\kappa}{\lambda} \end{pmatrix}$$

One can see that  $\epsilon$  also determines the mixing of singlet and non-singlet CP-even Higgs states. For small values of  $\epsilon$  and  $A_\kappa$ , characterizing the parameter space relevant to our study, the mass of the singlet CP-even Higgs boson is determined by  $2s\kappa = 2\mu\kappa/\lambda$ . This substantiates our earlier observation depicted in Fig. 1(a) and the relevance of the  $\mu\kappa/\lambda$  parameter used in our scan (Eq.). Further, in the sub-domain  $\mu\kappa/\lambda < 60$  GeV,  $h_1$  is light with  $m_{h_1} \simeq 2\mu\kappa/\lambda$  and has a significant singlet component, particularly for smaller values of  $\lambda$  (and  $A_\lambda$ ). In the upper sub-domain  $\mu\kappa/\lambda > 60$  GeV,  $h_1$  becomes the SM-like Higgs with  $m_{h_1} \simeq 120$  GeV while  $h_2$  acquires a large singlet component and mass  $m_{h_2} \simeq 2\mu\kappa/\lambda$ . This is illustrated in Fig. 2(b) showing the singlet fraction of  $h_1$ , the lightest CP-even Higgs boson.

To derive  $m_{a_1}$ , we diagonalize the  $\mathcal{M}_P$  matrix (Eq. 4). Keeping  $\mathcal{O}(\kappa)$ ,  $\mathcal{O}(\lambda^2)$ , and  $\mathcal{O}(\epsilon^2)$  terms, one has

$$m_{a_1}^2 = \frac{3}{2} (2\mu\kappa/\lambda)^2 (\zeta\lambda^2 - A_\kappa), \quad (9)$$

where  $\zeta = \frac{3}{2}v^2 \sin 2\beta/\mu$ . Because  $2\mu\kappa/\lambda$  determines the mass of the predominantly singlet CP-even Higgs boson,  $2\mu\kappa/\lambda \geq m_{h_1}$  and is always fairly large. Therefore,  $a_1$  is light if  $(\zeta\lambda^2 - A_\kappa)$  is low, motivating the choice of the empirical parameter  $(30 \text{ GeV})\lambda^2 - A_\kappa$  used in the scan. The range of this parameter selects a region with  $m_{a_1}$  between 0 and approximately 30 GeV, avoiding most of the theoretically inaccessible region in which  $\zeta\lambda^2 - A_\kappa < 0$  and therefore  $m_{a_1}^2 < 0$ , as shown in Fig. 1(b).

### Higgs Couplings and Decays

The couplings of  $h_1$  and  $a_1$  to each other and to Standard Model particles are determined primarily by their singlet and non-singlet components. While the CP-odd  $a_1$  is always nearly a pure singlet (see Fig. 2(a)), the singlet fraction of  $h_1$  is correlated with  $\mu\kappa/\lambda$ , but also depends on the smallness of  $\lambda$ . As illustrated by Fig. 2(b), for small  $\lambda$ ,  $h_1$  is nearly a pure singlet in the  $\mu\kappa/\lambda \lesssim 60$  GeV sub-region, while in the  $\mu\kappa/\lambda \gtrsim 60$  GeV domain,  $h_1$  has negligible singlet component and is essentially the SM Higgs. Figure 3 shows a strong suppression of reduced couplings of  $h_1$  to up- and down-type quarks as well as vector bosons in the  $\mu\kappa/\lambda \lesssim 60$  GeV domain. This suppression leads to a severe reduction in the production rates of  $h_1$  at colliders, making this scenario challenging for experimental exploration. Fortunately, as will be shown later, small  $\lambda$  values in the low  $\mu\kappa/\lambda$  region are excluded by cosmological observations.

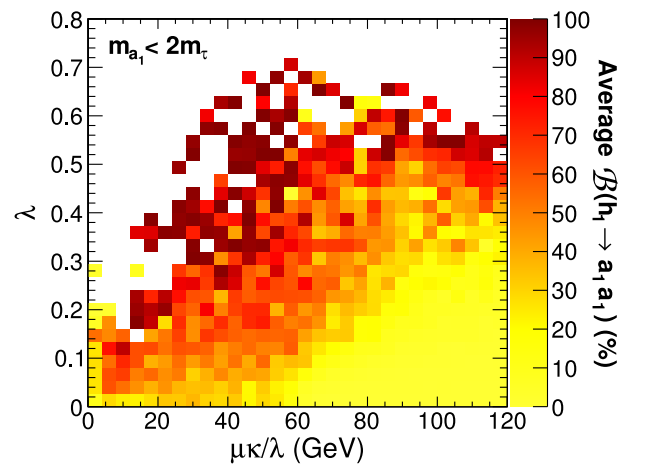


FIG. 4: Branching fraction of  $h_1 \rightarrow a_1 a_1$  in the  $\lambda$  versus  $\mu\kappa/\lambda$  plane, with the requirement that  $m_{a_1} < 2m_\tau$ .

Branching fractions of  $h_1$  are determined by relative strength of the  $h_1$  couplings to SM particles and the  $h_1 a_1 a_1$  coupling, which is specific to the NMSSM. Because  $a_1$  has a high singlet fraction, the singlet content of  $h_1$  is directly related to the strength of the  $h_1 a_1 a_1$  coupling. If this were the only effect,  $\mathcal{B}(h_1 \rightarrow a_1 a_1)$  would have been close to 100% in the lower half of the  $\mu\kappa/\lambda$  domain and negligible in the upper half. However, this coupling is also proportional to  $\lambda$  (see Eq. 2), which creates a competing effect as larger values of  $\lambda$  smear the nearly perfect separation of singlet- and doublet-type  $h_1$  in the lower and upper halves of the  $\mu\kappa/\lambda$  domain. The overall result is illustrated in Fig. 4, showing average  $\mathcal{B}(h_1 \rightarrow a_1 a_1)$  for NMSSM models with  $m_{a_1} < 2m_\tau$  as a function of  $\mu\kappa/\lambda$  and  $\lambda$ . It is evident that the suppression of  $h_1$  SM couplings for  $\mu\kappa/\lambda < 60$  GeV makes  $\mathcal{B}(h_1 \rightarrow a_1 a_1)$  substantial as long as  $\lambda$  is not too small. For the upper part of the  $\mu\kappa/\lambda$  domain,  $\mathcal{B}(h_1 \rightarrow a_1 a_1)$  is small except for large values of  $\lambda$  where the  $h_1$  singlet fraction is enhanced.

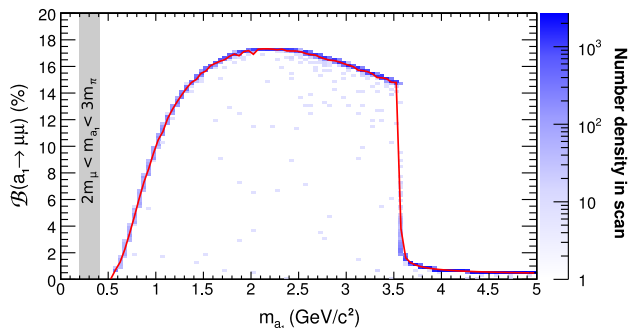


FIG. 5: Branching fraction of  $a_1 \rightarrow \mu\mu$  for generated models as a function of  $m_{a_1}$ . The red line is a mean of all scenarios as a function of  $m_{a_1}$ . The threshold at  $3.55$  GeV/ $c^2$  is  $2m_\tau$ . For  $2m_\mu < m_{a_1} < 3m_\pi$  (the grey box), the branching fraction would be nearly 100%.

As the lightest Higgs boson,  $a_1$  can only decay to SM particles, even though its coupling to SM particles is strongly suppressed due to its nearly singlet nature. One should also notice that  $a_1$  couplings to down-type fermions are proportional to  $\tan\beta$  while its couplings to up-type fermions are suppressed as  $1/\tan\beta$ . Therefore,  $a_1$  branching fractions follow the standard mass hierarchy of open decay channels to down-type fermions. Figure 5 shows the the branching fraction for  $a_1 \rightarrow \mu\mu$  as obtained using NMSSMTools package. For  $m_{a_1} < 2m_\tau$ , the  $a_1 \rightarrow \mu\mu$  channel becomes significant, making an analysis in the four-muon mode viable for experimental searches.

It is important to note that the NMSSMTools calculation of  $\mathcal{B}(a_1 \rightarrow \mu\mu)$  shown in Fig. 5 does not include hadronization effects important in the region  $m_{a_1} < 1$  GeV/ $c^2$ , and therefore is not reliable. One should also notice that for  $2m_\mu < m_{a_1} < 3m_\pi$ ,  $\mathcal{B}(a_1 \rightarrow \mu\mu)$  is expected to be about 100% because  $q\bar{q}$  and  $g g$  decays are

prohibited by hadronization and spin effects, and because  $\gamma\gamma$  is small. Since the status of  $\mathcal{B}(a_1 \rightarrow \mu\mu)$  in NMSSMTools for  $m_{a_1} < 0.5$  GeV/ $c^2$  is not well-established and requires further development, we present our results only for the  $m_{a_1} > 0.5$  GeV region. We would like to notice that  $\mathcal{B}(a_1 \rightarrow \mu\mu)$  is model-dependent in general and can be somewhat different in, for example, the Little Higgs model [38] used by the  $D\phi$  collaboration in Ref. [31]. Therefore, we present our results as limits on production cross-section times branching ratios for the  $4\mu$  signature as a model-independent limit for a given topology and signature under study.

## CURRENT EXPERIMENTAL CONSTRAINTS

Existing experimental data restrict the NMSSM parameter space for the scenario studied here. In the following, we discuss experimental measurements relevant to this scenario and evaluate their impact in restricting the allowed parameter space for models with low  $m_{a_1}$ .

### Cosmological Constraints

The lightest NMSSM neutralino is a candidate for Cold Dark Matter (CDM). The WMAP measurement of the CDM relic density therefore serves as an important constraint on the allowed NMSSM parameter space. In our scan, we used the MicrOmegas package [39] linked to NMSSMTools to calculate  $\Omega_{\text{NMSSM}} h^2$  and determine if a particular model is consistent with the experimental data. We considered a model to be consistent with the CDM measurement if  $\Omega_{\text{NMSSM}} h^2 \leq 0.1131 + 2 \times 0.0034$ , corresponding to the 95% upper limit obtained using the latest WMAP 5-year dataset [30]. The NMSSM neutralino relic density need not account for all CDM observed by WMAP, but it cannot exceed it.

To illustrate the effect of the WMAP constraints, Fig 6(a) shows the density of generated NMSSM models in the  $\lambda$  versus  $\mu\kappa/\lambda$  plane under the constraint that  $m_{a_1} < 2m_\tau$ . Models that were determined to be consistent with the WMAP data are shown in Fig. 6(b). The comparison shows that the WMAP bound excludes the region of small  $\mu\kappa/\lambda$  and  $\lambda$ . In that region, the lightest neutralino is light and weakly interacts with SM particles, suppressing the neutralino annihilation rate and enhancing the neutralino relic density to unacceptably large values. Figures 7(a) and (b) make the same comparison but in the  $m_{a_1}$  versus  $m_{h_1}$  plane.

### Constraints from Direct Searches at Colliders

Several searches for  $h_1 \rightarrow a_1 a_1$  have been performed at collider experiments, with the strongest impact on the



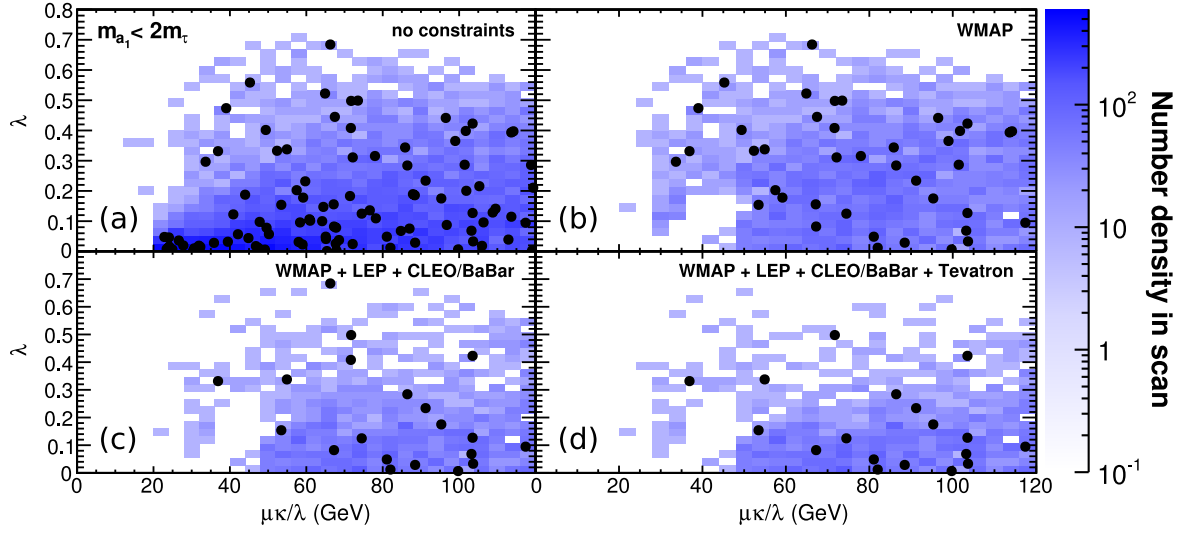


FIG. 6: Sampled points with  $m_{a_1} < 2m_\tau$  and experimental constraints successively applied in the  $\lambda$  vs.  $\mu\kappa/\lambda$  plane. The low energy  $e^+e^-$  data (CLEO and BaBar) have essentially no impact on the allowed parameter space. Color scale is number density and filled points are 100 models (before application of experimental constraints).

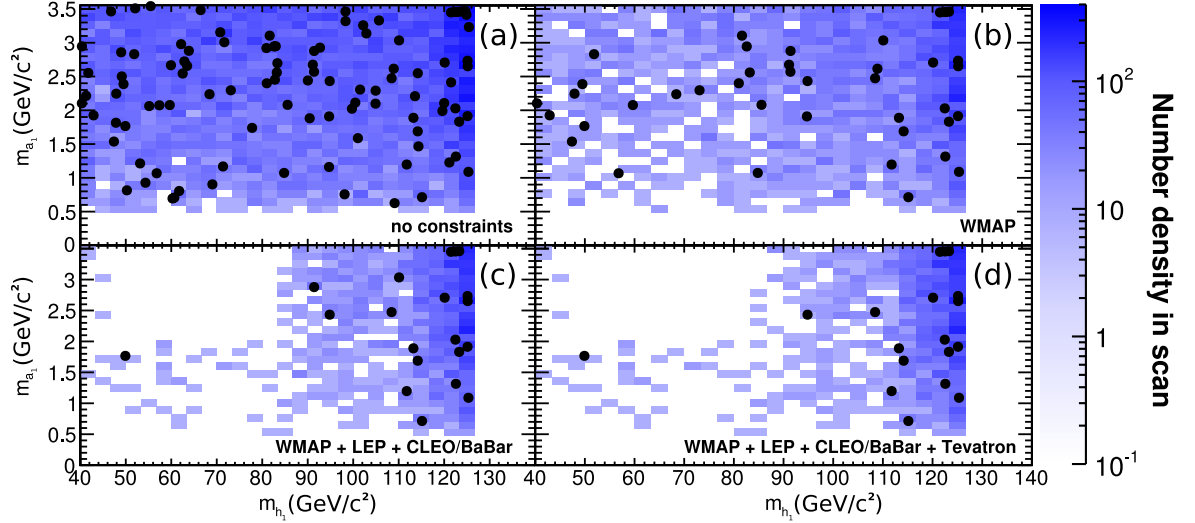


FIG. 7: Sampled points with  $m_{a_1} < 2m_\tau$  and experimental constraints successively applied similar to Fig. 6 but in the  $m_{a_1}$  vs.  $m_{h_1}$  plane. The low energy  $e^+e^-$  data (CLEO and BaBar) have essentially no impact on the allowed parameter space. Color scale is number density and filled points are 100 models (before application of experimental constraints).

allowed NMSSM models coming from LEP-II data [33]. Although the singlet component of  $h_1$  at low  $\mu\kappa/\lambda$  and  $\lambda$  (and correspondingly low  $m_{h_1}$ ) would severely suppress  $h_1$  production in  $e^+e^- \rightarrow h_1 Z$ , these extreme scenarios are excluded by the WMAP data. LEP limits [33] on NMSSM models are inferred from  $h_1 \rightarrow a_1 a_1$ ,  $a_1 \rightarrow$  pairs of charm, gluon, and  $\tau$  jets;  $a_1 \rightarrow \mu\mu$  limits were not quoted. The LEP-II upper limit on  $e^+e^- \rightarrow h_1 Z$  with  $h_1 \rightarrow a_1 a_1$  excludes models that predict  $m_{h_1}$  within the kinematic limits,  $45 < m_{h_1} < 86$  GeV/ $c^2$ , and  $m_{a_1}$  in the region of significant detector efficiency,  $m_{a_1} > 2$  GeV/ $c^2$ .

In addition to LEP data, there were direct searches for

$\Upsilon \rightarrow \gamma a_1$  by CLEO and BaBar at low energy  $e^+e^-$  colliders [40, 41]. Neither of these searches significantly constrain the NMSSM models with low  $m_{a_1}$  because  $a_1$  has a high singlet component, and thus negligible  $bb a_1$  coupling (see Fig. 2(a)), for all sampled parameter values. Because CLEO and BaBar results have negligible effect on the allowed parameter space, Figs. 6(c) and 7(c) show combined LEP+CLEO+BaBar constraints, but the reader is reminded that only LEP constraints are relevant.

The flat  $\ell^+\ell^-$  distribution of rare  $B \rightarrow K \ell^+\ell^-$  decays [42] could potentially set a limit on the parameter space under study through the bound on  $\mathcal{B}(B \rightarrow K a_1) \times$

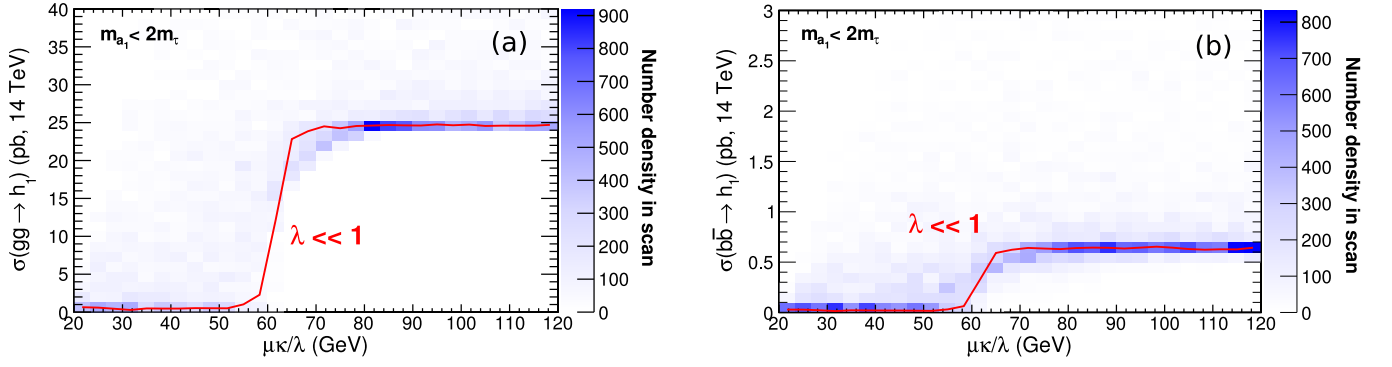


FIG. 8: Contributions to the  $pp \rightarrow h_1$  production cross-section at  $\sqrt{s} = 14$  TeV as a function of  $\mu\kappa/\lambda$  and  $\lambda$ , from  $gg$  (a) and  $b\bar{b}$  (b), with the requirement that  $m_{a_1} < 2m_\tau$ . (The red line is a mean of  $\lambda < 0.01$  scenarios.)

$\mathcal{B}(a_1 \rightarrow \mu\mu)$ . However, this limit does not actually bound the region of our interest because the coupling of  $a_1$  to up-type and down-type quarks in  $b \rightarrow sa_1$  penguin diagrams is suppressed due to the highly singlet nature of  $a_1$ . For  $f_a = \tan\theta_P v \sin(2\beta)/2$ , the quantity  $f_a \tan^2\beta$  is above 100 TeV in our scan while the charged Higgs mass is typically above 200 GeV/ $c^2$ . Thus, the bound set in Fig. 2 of Ref. [36] is not relevant to the parameter space of our study.

The results of a search [43] for the NMSSM with a low mass  $a_1$  at the Tevatron was recently published by the  $D\phi$  collaboration in the channel  $h_1 \rightarrow a_1 a_1 \rightarrow 4\mu$ . With no excess of data over the SM expectations, the paper quotes 95% C.L. upper limits for the cross-section of this process. To interpret the  $D\phi$  result in terms of constraints on allowed NMSSM models in our scan, we calculate the NLO production cross-section for  $p\bar{p} \rightarrow h_1$  in the NMSSM using the SM NLO calculations for  $gg \rightarrow H_{SM}$  [44] and  $b\bar{b} \rightarrow H_{SM}$  with QCD-improved (running) Yukawa couplings [45], corrected for differences in coupling between the SM and the NMSSM using NMSSMTools:

$$\sigma(gg \rightarrow h_1) = \sigma(gg \rightarrow H_{SM}) \frac{\Gamma(h_1 \rightarrow gg)}{\Gamma(H_{SM} \rightarrow gg)} \quad (10)$$

$$= \sigma(gg \rightarrow H_{SM}) \frac{Br(h_1 \rightarrow gg) \Gamma^{\text{tot}}(h_1)}{\Gamma(H_{SM} \rightarrow gg)} \quad (11)$$

where  $\sigma(gg \rightarrow H_{SM})$  and  $\Gamma(H_{SM} \rightarrow gg)$  are calculated using HIGLU [46], while  $\mathcal{B}(h_1 \rightarrow gg)$ ,  $\Gamma^{\text{tot}}(h_1)$ , and the ratio of Yukawa couplings  $Y_{bbh_1}/Y_{bbH_{SM}}$  are obtained using NMSSMTools. For  $\mu\kappa/\lambda < 60$  GeV (non-SM  $h_1$  lighter than 120 GeV/ $c^2$ ), the cross-section is strongly suppressed even compared to the SM for low  $m_{a_1}$  because  $h_1$  has a large singlet fraction and weakly couples to SM particles (see Fig. 3). For larger  $\mu\kappa/\lambda$ , the lightest CP-even Higgs  $h_1$  becomes the SM-like Higgs and has a small  $h_1 \rightarrow a_1 a_1$  branching fraction.

The  $D\phi$  paper [43] quotes 95% C.L. limits on

$\sigma(p\bar{p} \rightarrow h_1) \times B(h_1 \rightarrow a_1 a_1 \rightarrow 4\mu)$  for several choices of  $m_{a_1}$  with  $m_{h_1} = 100$  GeV/ $c^2$ . To determine if a particular model in our scan is excluded by these data, we linearly interpolate the published cross-section limits for values of  $m_{a_1}$  between the points in [43]. To obtain the experimental cross-section limits as a function of  $m_{h_1}$ , we need to correct for variations in the experimental acceptance. We obtain those limits by taking the analysis acceptance to be linear as a function of  $m_{h_1}$  “increasing by  $\sim 10\%$  when  $m_{h_1}$  increases from 80 to 150 GeV/ $c^2$ ” [43] and matching it to the full analysis acceptance given at  $m_{h_1} = 100$  GeV/ $c^2$ . We then calculate the production cross-section and branching fractions for the model points and compare them to the values we derive from [43]. Figures 6(d) and 7(d) show the density of NMSSM models surviving WMAP, LEP and Tevatron constraints. Because of the suppression in production rate at low  $\mu\kappa/\lambda$  and small  $\mathcal{B}(h_1 \rightarrow a_1 a_1)$  at high  $\mu\kappa/\lambda$ , the Tevatron search has only a limited impact on the allowed NMSSM parameter space, mainly excluding models with high  $\lambda$ . A significant improvement in Tevatron reach for the NMSSM would require a large increase in integrated luminosity, thus requiring the LHC to make a definitive discovery or exclusion of NMSSM models with low  $m_{a_1}$ .

## A DEDICATED SEARCH FOR THE LOW- $m_{a_1}$ NMSSM AT THE LHC

Since  $a_1$  is only weakly coupled to SM particles, it can only be produced at the LHC via decays of the lightest scalar Higgs  $h_1 \rightarrow a_1 a_1$ . The main characteristic of such signal at the LHC is two back-to-back (in  $\phi$ ) di-muon pairs of spatially nearby muons. The reconstructed di-muon pairs should have invariant masses consistent with one another, and their invariant masses also serve as a direct measurement of  $m_{a_1}$ . Additionally, the  $4\mu$  invariant mass distribution should have a narrow peak corresponding to the  $m_{h_1}$  mass. We use these striking features to design an analysis suitable for early LHC running.

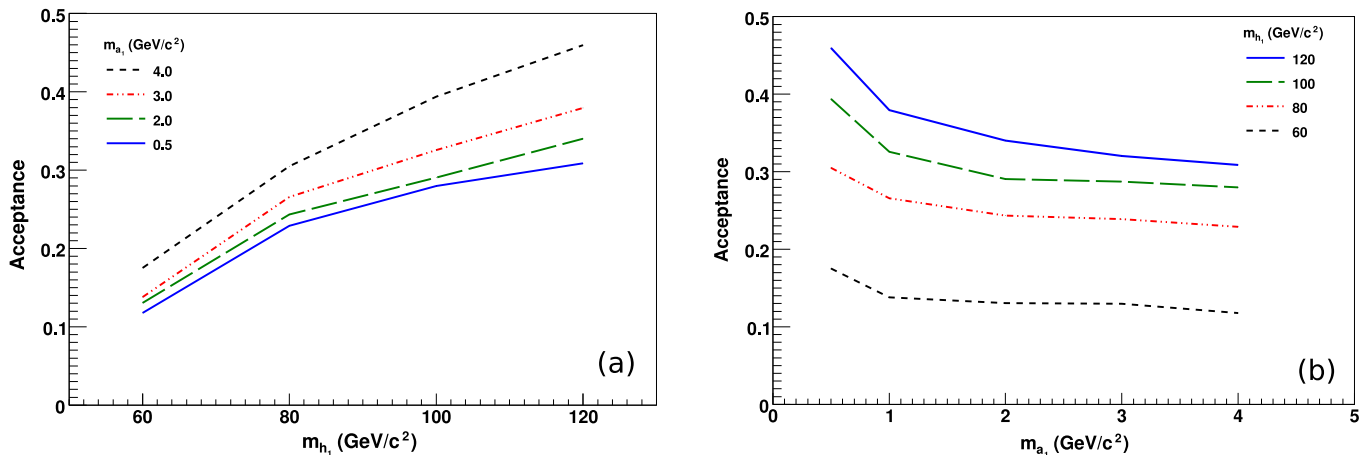


FIG. 9: (a): Acceptance as a function of  $m_{a_1}$  for fixed  $m_{h_1}$ . (b): Acceptance as a function of  $m_{h_1}$  for fixed  $m_{a_1}$ .

The four-muon final state considered in this analysis has relatively low experimental backgrounds. Therefore, instead of using the Vector Boson Fusion (VBF) production process chosen in the proposed NMSSM searches targeting the  $m_{a_1} > 2m_\tau$  region [25], we focus on the largest Higgs production modes at the LHC,  $gg \rightarrow h_1$  and  $b\bar{b} \rightarrow h_1$ . We calculate the NLO cross-section for  $pp \rightarrow h_1$  for the NMSSM by rescaling the LHC SM NLO calculations [44, 45] to correct for differences in couplings between the SM and NMSSM (Eqs. 10 and 11). Like the Tevatron case, the cross-section is strongly suppressed compared to the SM if  $h_1$  has a large singlet fraction. Figure 8 shows the production cross-section for 14 TeV  $pp \rightarrow h_1 + X$  as a function of  $\mu\kappa/\lambda$ . While this suppression makes the analysis challenging even at the LHC, the constraints arising from the WMAP relic density measurement exclude models with very low values of  $\lambda$ , so the allowed models have small but non-negligible production cross-section.

### Analysis Selections

We use Pythia to generate signal event templates with  $m_{h_1}$  in the range from 70 to 140 GeV/c<sup>2</sup> and  $m_{a_1}$  in the range from 0.5 to 4 GeV/c<sup>2</sup>. We chose the CMS detector as a benchmark for modeling a realistic experimental environment, with parameters described in Ref. [47]. The important parameters for this analysis are muon momentum resolution, the minimum muon momentum needed to reach the muon system, geometric acceptance, and the average muon reconstruction efficiencies. Because of the large number of reconstructed muons in the event, we take the trigger efficiency to be 100%.

The analysis starts by requiring at least four muon candidates with transverse momentum  $p_T > 5$  GeV/c and pseudorapidity  $|\eta| < 2.4$  to ensure high and reli-

able reconstruction efficiency. Of the four muon candidates, at least one must have  $p_T > 20$  GeV/c to suppress major backgrounds and to satisfy trigger requirements. Each event is required to have at least two positively charged and two negatively charged muon candidates. For the surviving events, we define quadruplets of candidates, pairing the candidates by charge and sorting them into two di-muon pairs by minimizing the quantity  $(\Delta R(\mu_i, \mu_j)^2 + \Delta R(\mu_k, \mu_l)^2)$ , where  $\Delta R^2 = \Delta\eta^2 + \Delta\phi^2$ . Muon quadruplets for which  $\Delta R > 0.5$  in either of the pairs are discarded as inconsistent with the signal topology. Acceptance for the selections listed above is shown in Fig. 9 for several representative values of  $m_{h_1}$  and  $m_{a_1}$ .

The requirement of four sufficiently energetic muons in the event dramatically reduces contributions of potential backgrounds for this analysis. After acceptance selections, the dominant background is due to the QCD multijet production where muons originate from heavy-flavor resonances, heavy-flavor quark decays, or from  $\pi/K$  decays-in-flight. We use Pythia to estimate the QCD multijet background, and obtain approximately 2.6 events/pb<sup>-1</sup> (approximately half containing at least one decay-in-flight). Using CalcHEP [48] to estimate  $pp \rightarrow 4\ell + X$  electroweak backgrounds, we obtain 0.04 events/pb<sup>-1</sup>. Direct  $J/\psi$  production is found by Pythia to be completely negligible. Other SM backgrounds (top, W+jets) are negligible in the region of interest of this analysis.

The backgrounds are further reduced by requiring the kinematics to be consistent with the expected signal signature. We calculate the invariant mass of each of di-muon pair,  $m_{12}$  and  $m_{34}$ , as well as the invariant mass of all four muons, denoted as  $m_{1234}$ . Figure 10(a) shows the invariant mass of the muon pairs passing all selections in signal events for two choices of  $m_{h_1}$  and  $m_{a_1}$ . Figure 10(b) shows the distribution of  $m_{1234}$  for two benchmark points. To focus on the region of interest, we re-



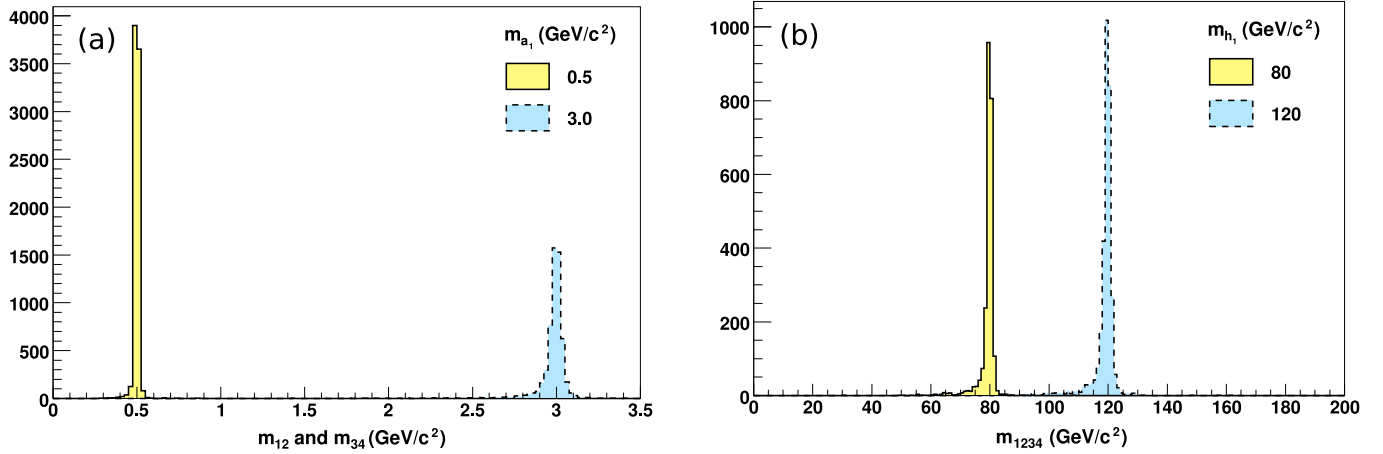


FIG. 10: (a): Invariant mass of reconstructed muon pairs for  $m_{a_1} = 0.5$  and  $3 \text{ GeV}/c^2$  (in both cases  $m_{h_1} = 100 \text{ GeV}/c^2$ ). (b): Invariant mass of four reconstructed muons for  $m_{h_1} = 80$  and  $120 \text{ GeV}/c^2$  (in both cases  $m_{a_1} = 3.0 \text{ GeV}/c^2$ ).

quire  $m_{1234} > 60 \text{ GeV}/c^2$ ,  $m_{12}, m_{34} < 4 \text{ GeV}/c^2$ , which reduces the QCD background to  $0.4 \text{ events}/\text{pb}^{-1}$ .

To ensure the compatibility of the measured invariant masses of the two di-muon pairs, one could require  $|m_{12} - m_{34}| < 0.08 + 0.005 \times (m_{12} + m_{34})$ . Such cut would require the two pair masses to be consistent with each other and would take into account the widening of absolute resolution in the reconstructed di-muon mass as a function of mass. If applied, the only background that still may be not completely negligible is the QCD multi-jet production, for which we conservatively estimate the upper bound to be  $0.02 \text{ events}/\text{pb}^{-1}$ . However, instead of applying this selection explicitly, a better approach would be to fit the data in the 3D space  $(m_{12}, m_{34}, m_{1234})$ , taking into account kinematic properties of the signal events. This approach maximizes the signal acceptance and therefore the statistical power of the analysis. It is also convenient from an experimental standpoint as the background events are distributed smoothly over the 3D space, allowing a fit of the 3D distribution to estimate backgrounds directly from the data. A potential signal would appear as a concentration of events in a small region of the space (a 3D peak). We use a binned likelihood defined as a function of parameters  $m_{a_1}$ ,  $m_{h_1}$  and effective signal cross-section  $\sigma \times \mathcal{B}(h_1 \rightarrow a_1 a_1) \mathcal{B}^2(a_1 \rightarrow \mu\mu)$  to fit the simulated data using either background-only or signal-plus-background templates. We estimate the sensitivity of this analysis and present it in terms of the 95% C.L. exclusion levels for signal cross-section using a Bayesian technique.

Our estimations show that for an early data search ( $\mathcal{L} \simeq 100 \text{ pb}^{-1}$ ), the backgrounds are negligible. For an analysis with higher luminosity, one can restore the zero-background situation by adding an isolation requirement to one or both of the di-muon pairs in the event. Isolation can be defined by either setting an upper bound

TABLE I: Expected rate of background events per  $100 \text{ pb}^{-1}$  of luminosity after selection.

Selection	4 leptons	QCD multi-jet
$p_T(\mu_1) > 20 \text{ GeV}/c$ and $p_T(\mu_i) > 5 \text{ GeV}/c; i = 2, 3, 4$	$4.8 \pm 0.2$	$267 \pm 23$
$m_{12}, m_{34} < 4 \text{ GeV}/c^2$	$0.024 \pm 0.012$	$90 \pm 13$
$m_{1234} > 60 \text{ GeV}/c^2$	$0.010 \pm 0.007$	$39 \pm 9$
$ m_{12} - m_{34}  < 0.08 \text{ GeV}/c^2$ $+ 0.005 \times (m_{12} + m_{34})$	$0.000^{+0.005}_{-0.000}$	$0.00^{+1.95}_{-0.00}$

on the sum of the transverse momenta of all tracks in a cone around the reconstructed direction of the di-muon pair, excluding two muon tracks, or by rejecting pairs with additional tracks above a certain threshold. For the analysis with  $\mathcal{L} = 1 \text{ fb}^{-1}$  of data, we required no charged tracks with momentum  $p_T > 1 \text{ GeV}/c$  in the  $\sqrt{(\Delta\eta)^2 + (\Delta\phi)^2} < 0.3$  cone around the direction of at least one of the two muon pairs. This requirement is 96% efficient for signal and reduces QCD multijet background, dominated by events with muons originating from heavy flavor jets, by a factor of 6–7. For high-luminosity datasets, isolation can be further tightened to increase background suppression with only a moderate loss in signal efficiency.

#### LHC Reach for NMSSM $h_1 \rightarrow a_1 a_1$

We have proposed an analysis that has a potential of discovering the NMSSM with early LHC data in scenarios with low  $m_{a_1}$ . We estimate its sensitivity by

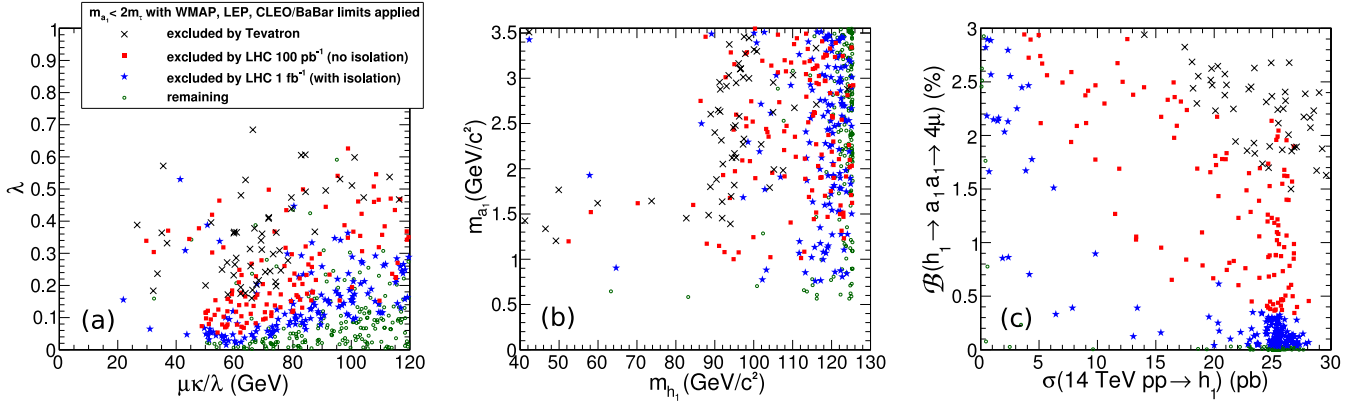


FIG. 11: Sampled models with  $m_{a_1} < 2m_\tau$  and all experimental constraints applied, presented as a function of model parameters (a), Higgs masses (b), branching fraction and LHC cross-section (c). With only  $100 \text{ pb}^{-1}$ , the LHC's reach extends beyond that of the Tevatron.

calculating the 95% C.L. upper limit on the product  $\sigma(pp \rightarrow h) \mathcal{B}(h_1 \rightarrow a_1 a_1) \mathcal{B}^2(a_1 \rightarrow \mu\mu) \alpha$ , where  $\alpha$  is the analysis acceptance, using a Bayesian technique. Because of the low background, an upper limit on the signal corresponds to approximately three reconstructed events. This limit is  $0.0293 \text{ pb}$  for  $\mathcal{L} = 100 \text{ pb}^{-1}$ , and scales linearly with luminosity assuming that the number of observed background events is zero. In nearly all pseudoexperiments, this limit is independent of  $m_{h_1}$  and  $m_{a_1}$  because the effective signal region that dominates signal significance is essentially background-free and the probability to observe an event is small. Note that the corresponding projection for  $\mathcal{L} = 1 \text{ fb}^{-1}$  includes the isolation cut, slightly reducing signal efficiency and correspondingly loosening the limit. The upper limit on  $\sigma(pp \rightarrow h_1) \mathcal{B}(h_1 \rightarrow a_1 a_1)$  is shown as a function of  $m_{h_1}$  and  $m_{a_1}$  in Table II.

Figure 11 presents the region of NMSSM parameter space excluded by the Tevatron and the region that the LHC would exclude with  $100 \text{ pb}^{-1}$  (without isolation) and  $1 \text{ fb}^{-1}$  (with isolation), assuming no observed signal. The regions are presented in the  $\lambda$ ,  $\mu\kappa/\lambda$  plane (Fig. 11(a)), the  $m_{a_1}$ ,  $m_{h_1}$  plane (Fig. 11(b)), and the plane of  $h_1 \rightarrow a_1 a_1 \rightarrow 4\mu$  branching fraction versus LHC  $pp \rightarrow h_1$  cross-section (Fig. 11(c)). High  $h_1$ -singlet scenarios (which have low production cross-section) and low  $h_1$ -singlet scenarios (which have low  $h_1 \rightarrow a_1 a_1$  branching fractions) are accessible to the Tevatron and the LHC to different degrees, leading to a region in Fig. 11(c) where high  $h_1$ -singlet scenarios are excluded by the Tevatron while some low  $h_1$ -singlet models with the same LHC cross-section times branching fraction are not. The Tevatron exclusion region has a sharp border only when viewed as a function of the Tevatron cross-section.

It is worth noting that quantitative background estimates performed in our analysis may indicate that the LHC reach for NMSSM models with  $m_{a_1} > 2m_\tau$  in the  $2\mu 2\tau$  channel are substantially weaker than suggested

TABLE II: 95% C.L. upper limit on  $\sigma(pp \rightarrow h_1) \times \mathcal{B}(h_1 \rightarrow a_1 a_1 \rightarrow 4\mu)$  (fb) at the LHC with  $\mathcal{L} = 100 \text{ pb}^{-1}$  (no isolation) and  $\mathcal{L} = 1 \text{ fb}^{-1}$  (with isolation). The limit tightens at high  $m_{h_1}$  because of the increase in acceptance with  $m_{h_1}$ .

	$m_{a_1} \text{ (GeV}/c^2\text{)}$				
	0.5	1.0	2.0	3.0	4.0
$\mathcal{B}(a_1 \rightarrow \mu\mu) \text{ (%)}$	0 <sup>a</sup>	9.8	15.2	16.2	0.7
for $\mathcal{L} = 100 \text{ pb}^{-1}$ (no isolation)					
$m_{h_1} = 80 \text{ GeV}/c^2$	96.0	110.3	121.1	122.6	126.1
$m_{h_1} = 100 \text{ GeV}/c^2$	74.8	90.3	100.8	102.4	103.9
$m_{h_1} = 120 \text{ GeV}/c^2$	63.9	77.4	86.0	90.8	94.4
for $\mathcal{L} = 1000 \text{ pb}^{-1}$ (with isolation)					
$m_{h_1} = 80 \text{ GeV}/c^2$	10.0	11.5	12.6	12.8	13.1
$m_{h_1} = 100 \text{ GeV}/c^2$	7.8	9.4	10.5	10.7	10.8
$m_{h_1} = 120 \text{ GeV}/c^2$	6.7	8.1	9.0	9.5	9.8

<sup>a</sup>Recall that  $\mathcal{B}(h_1 \rightarrow a_1 a_1)$  is obtained using NMSSMTools and is not reliable for  $m_{a_1} \lesssim 1 \text{ GeV}/c^2$ . Furthermore, this branching fraction is expected to reach nearly 100% for  $2m_\mu < m_{a_1} < 3m_\tau$ .

in Ref. [26], which relied on extrapolating QCD backgrounds to avoid high-statistics simulations. Though the  $4\mu$  and  $2\mu 2\tau$  analyses apply different selections, a rough extrapolation of the simulated QCD multijet backgrounds to the  $4\mu$  channel yields an estimate of backgrounds to the  $2\mu 2\tau$  channel that is three orders of magnitude larger than what was used in Ref. [26], even without considering the much larger misidentification rate of hadronically decaying taus. The expected number of QCD multijet events in the  $m_{1234} > 60$ ,  $m_{12}$  and  $m_{34} < 4 \text{ GeV}/c^2$  region of the  $4\mu$  analysis, which is  $390 \pm 90 \text{ events}/\text{fb}^{-1}$  (note that the numbers in Table I

are for  $100 \text{ pb}^{-1}$ ), could be reduced by a factor of 10–20 using tight isolation requirements. Unlike our analysis, the study in Ref. [26] applies restrictions on the transverse momentum of the di-muon pair,  $p_T^{\mu\mu} > 40 \text{ GeV}/c$ , and on the missing transverse energy  $\cancel{E}_T > 30 \text{ GeV}$ . However, the  $p_T^{\mu\mu}$  selection is similar to  $m_{1234} > 60 \text{ GeV}/c^2$  and, given typical expected  $\cancel{E}_T$  resolution for multi-jet events, a  $\cancel{E}_T > 30 \text{ GeV}$  requirement cannot be powerful enough to overcome several orders of magnitude in estimated event count. Scaling the  $4\mu$  background estimate down by a factor of 10 to account for muon isolation, we expect about  $39 \pm 9 \text{ events}/\text{fb}^{-1}$  from QCD multijets, as opposed to the  $0.03 \text{ events}/\text{fb}^{-1}$  in Ref. [26]. Allowing for the larger rate of tau misidentification compared to muons only increases the discrepancy. Another argument can be made using the  $D\bar{O}$  measurement in the  $2\mu 2\tau$  channel [43], which had 1–2 expected background events in the narrow ( $\pm 0.3$ – $1.0 \text{ GeV}/c^2$ ) windows around the selected points in the di-muon mass. Using common scaling estimates of background contributions from the Tevatron to the LHC, one would expect similar backgrounds for LHC datasets of the order of  $100 \text{ pb}^{-1}$ . For datasets with integrated luminosities of the order of  $500 \text{ pb}^{-1}$ , the corresponding QCD contamination would be 5–10 events per window. These much larger background estimates severely affect achievable exclusion limits and, considering trial factors, would make any discovery in the  $2\mu 2\tau$  channel with early data extremely challenging.

## CONCLUSIONS

We have studied the phenomenology of the NMSSM scenarios with the mass of the lowest CP-odd Higgs boson,  $a_1$ , below the  $2\tau$  threshold. Our analysis of the impact of existing data on these models has shown that the WMAP and LEP-II data provide the most constraining power, while recent CLEO and BaBar measurements have essentially no impact on the allowed parameter space, and the Tevatron data has only a weak impact on the allowed parameter space. As a result, a large fraction of the parameter space is not excluded by any existing data. We conclude that a new analysis should be performed at the LHC to definitively confirm or exclude these models. We propose an analysis suitable for the LHC using the  $4\mu$  signature, which has very low backgrounds and striking kinematical features allowing direct and precise measurement of the masses of the  $a_1$  and  $h_1$  bosons. Using the CMS experiment as a benchmark, we estimate the sensitivity of such an analysis and demonstrate that it has the potential to either make a discovery or significantly diminish the allowed parameter space of the NMSSM with low  $m_{a_1}$  using only  $100$ – $1000 \text{ pb}^{-1}$  of early LHC data.

## Acknowledgments

We thank Ulrich Ellwanger, Cyril Hugonie, Alexander Pukhov, Jay Wacker for useful discussions. One of the authors (AB) would like to thank the GGI Institute (Florence), and another (JP) would like to thank Fermilab, where important parts of the work on the paper were performed. This work would not be possible without the support of the U.S. Department of Energy, the State of Texas, and the Universities Research Association Visiting Scholars Program.

- 
- [1] H. P. Nilles, M. Srednicki and D. Wyler, Phys. Lett. B **120** (1983) 346.
  - [2] J. M. Frere, D. R. T. Jones and S. Raby, Nucl. Phys. B **222** (1983) 11.
  - [3] J. R. Ellis, J. F. Gunion, H. E. Haber, L. Roszkowski and F. Zwirner, Phys. Rev. D **39** (1989) 844.
  - [4] M. Drees, Int. J. Mod. Phys. A **4** (1989) 3635.
  - [5] U. Ellwanger, Phys. Lett. B **303** (1993) 271 [arXiv:hep-ph/9302224].
  - [6] U. Ellwanger, M. Rausch de Traubenberg and C. A. Savoy, Phys. Lett. B **315** (1993) 331 [arXiv:hep-ph/9307322].
  - [7] T. Elliott, S. F. King and P. L. White, Phys. Rev. D **49** 2435 (1994) 2435 [arXiv:hep-ph/9308309].
  - [8] P. N. Pandita, Z. Phys. C **59** (1993) 575.
  - [9] U. Ellwanger, M. Rausch de Traubenberg and C. A. Savoy, Z. Phys. C **67** (1995) 665 [arXiv:hep-ph/9502206].
  - [10] S. F. King and P. L. White, Phys. Rev. D **52** (1995) 4183 [arXiv:hep-ph/9505326].
  - [11] F. Franke and H. Fraas, Int. J. Mod. Phys. A **12** (1997) 479 [arXiv:hep-ph/9512366].
  - [12] U. Ellwanger, M. Rausch de Traubenberg and C. A. Savoy, Nucl. Phys. B **492** (1997) 21 [arXiv:hep-ph/9611251].
  - [13] D. J. Miller, R. Nevzorov and P. M. Zerwas, Nucl. Phys. B **681** (2004) 3.
  - [14] J. E. Kim and H. P. Nilles, Phys. Lett. B **138**, 150 (1984).
  - [15] R. Dermisek and J. F. Gunion, Phys. Rev. Lett. **95**, 041801 (2005) [arXiv:hep-ph/0502105].
  - [16] A. Menon, D. E. Morrissey and C. E. M. Wagner, Phys. Rev. D **70** (2004) 035005 [arXiv:hep-ph/0404184]; D. G. Cerdeno, C. Hugonie, D. E. Lopez-Fogliani, C. Munoz and A. M. Teixeira, JHEP **0412** (2004) 048 [arXiv:hep-ph/0408102]; G. Belanger, F. Boudjema, C. Hugonie, A. Pukhov and A. Semenov, JCAP **0509**, 001 (2005) [arXiv:hep-ph/0505142]; J. F. Gunion, D. Hooper and B. McElrath, Phys. Rev. D **73**, 015011 (2006) [arXiv:hep-ph/0509024]; F. Ferrer, L. M. Krauss and S. Profumo, Phys. Rev. D **74**, 115007 (2006) [arXiv:hep-ph/0609257]; D. G. Cerdeno, E. Gabrielli, D. E. Lopez-Fogliani, C. Munoz and A. M. Teixeira, JCAP **0706**, 008 (2007) [arXiv:hep-ph/0701271]; C. Hugonie, G. Belanger and A. Pukhov, JCAP **0711**, 009 (2007) [arXiv:0707.0628 [hep-ph]]; V. Barger, P. Langacker, I. Lewis, M. McCaskey, G. Shaughnessy and B. Yencho, Phys. Rev. D **75**, 115002

- (2007) [arXiv:hep-ph/0702036]. S. Kraml, A. R. Raklev and M. J. White, Phys. Lett. B **672**, 361 (2009) [arXiv:0811.0011 [hep-ph]]; G. Belanger, C. Hugonie and A. Pukhov, JCAP **0901**, 023 (2009) [arXiv:0811.3224 [hep-ph]].
- [17] B. A. Dobrescu, G. L. Landsberg and K. T. Matchev, Phys. Rev. D **63**, 075003 (2001) [arXiv:hep-ph/0005308]; B. A. Dobrescu and K. T. Matchev, JHEP **0009**, 031 (2000) [arXiv:hep-ph/0008192].
- [18] J. F. Gunion, H. E. Haber and T. Moroi, *In the Proceedings of 1996 DPF / DPB Summer Study on New Directions for High-Energy Physics (Snowmass 96), Snowmass, Colorado, 25 Jun - 12 Jul 1996, pp LTH095* [arXiv:hep-ph/9610337]; U. Ellwanger, J. F. Gunion and C. Hugonie, arXiv:hep-ph/0111179
- [19] J. R. Ellis, J. F. Gunion, H. E. Haber, L. Roszkowski and F. Zwirner, Phys. Rev. D **39**, 844 (1989); B. A. Dobrescu, G. L. Landsberg and K. T. Matchev, Phys. Rev. D **63**, 075003 (2001) [arXiv:hep-ph/0005308]; U. Ellwanger, J. F. Gunion, C. Hugonie and S. Moretti, arXiv:hep-ph/0305109; U. Ellwanger, J. F. Gunion, C. Hugonie and S. Moretti, arXiv:hep-ph/0401228; U. Ellwanger, J. F. Gunion and C. Hugonie, JHEP **0507**, 041 (2005) [arXiv:hep-ph/0503203].
- [20] S. Moretti, S. Munir and P. Poulose, Phys. Lett. B **644**, 241 (2007) [arXiv:hep-ph/0608233];
- [21] S. Chang, P. J. Fox and N. Weiner, Phys. Rev. Lett. **98**, 111802 (2007) [arXiv:hep-ph/0608310].
- [22] R. Dermisek and J. F. Gunion, Phys. Rev. D **75**, 075019 (2007) [arXiv:hep-ph/0611142].
- [23] K. Cheung, J. Song and Q. S. Yan, Phys. Rev. Lett. **99**, 031801 (2007) [arXiv:hep-ph/0703149].
- [24] J. R. Forshaw, J. F. Gunion, L. Hodgkinson, A. Papaefstathiou and A. D. Pilkington, JHEP **0804** (2008) 090 [arXiv:0712.3510 [hep-ph]].
- [25] A. Belyaev, S. Hesselbach, S. Lehti, S. Moretti, A. Nikitenko and C. H. Shepherd-Themistocleous, arXiv:0805.3505 [hep-ph].
- [26] Mariangela Lisanti, Jay G. Wacker, Published in Phys. Rev. D **79**:115006, (2009), arXiv:0903.1377;
- [27] U. Ellwanger, J.F. Gunion and C. Hugonie, JHEP **0502**, 066 (2005).
- [28] U. Ellwanger, C. Hugonie, Comput. Phys. Commun. **175**, 290 (2006).
- [29] F. Domingo and U. Ellwanger, arXiv:0710.3714 [hep-ph].
- [30] D. N. Spergel *et al.* [WMAP Collaboration], Astrophys. J. Suppl. **148**, 175 (2003) [arXiv:astro-ph/0302209]; C. L. Bennett *et al.* [WMAP Collaboration], Astrophys. J. Suppl. **148**, 1 (2003) [arXiv:astro-ph/0302207]; D. N. Spergel *et al.* [WMAP Collaboration], Astrophys. J. Suppl. **170**, 377 (2007) [arXiv:astro-ph/0603449]. X. X. X *et al.* [WMAP Collaboration], [arXiv:astro-ph/0803.0547].
- [31] V. M. Abazov *et al.* [D0 Collaboration], Phys. Rev. Lett. **103**, 061801 (2009) [arXiv:0905.3381 [hep-ex]].
- [32] G. Abbiendi *et al.* (OPAL Collaboration), Eur. Phys. J. C **18**, 425-445 (2001).
- [33] G. Abbiendi *et al.* (OPAL Collaboration), Eur. Phys. J. C **27**, 483-495 (2003), arXiv:0209068v1 [hep-ex].
- [34] W. Love *et al.* [CLEO Collaboration], Phys. Rev. Lett. **101**, 151802 (2008) [arXiv:0807.1427 [hep-ex]].
- [35] B. Aubert *et al.* [BABAR Collaboration], Phys. Rev. Lett. **103**, 081803 (2009) [arXiv:0905.4539 [hep-ex]].
- [36] M. Freytsis, Z. Ligeti and J. Thaler, arXiv:0911.5355 [hep-ph].
- [37] U. Ellwanger, C. Hugonie and A. M. Teixeira, arXiv:0910.1785 [hep-ph].
- [38] K. Cheung, J. Song, P. Tsong, Q.-S. Yan, Phys. Rev. D **78**, 055015 (2008), arXiv:hep-ph/0806.4411;
- [39] G. Belanger, F. Boudjema, C. Hugonie, A. Pukhov, A. Semenov, JCAP **0509**:001 (2005), arXiv:hep-ph/0505142
- [40] D. Besson *et al.* (CLEO Collaboration) Phys. Rev. D **76**, 117102 (2007);
- [41] B. Aubert *et al.* (BaBar Collaboration), PRL **103**, 081803 (2009);
- [42] I. Adachi *et al.* [Belle Collaboration], arXiv:0810.0335 [hep-ex].
- [43] V.M. Abazov *et al.* (D0 Collaboration), PRL **103**, 061801 (2009).
- [44] M. Spira, A. Djouadi, D. Graudenz and P. M. Zerwas, Nucl. Phys. B **453**, 17 (1995) [arXiv:hep-ph/9504378].
- [45] C. Balazs, H. J. He and C. P. Yuan, Phys. Rev. D **60**, 114001 (1999) [arXiv:hep-ph/9812263].
- [46] M. Spira, NIMA **389**, 1997 (357) [arXiv:hep-ph/9610350].
- [47] (CMS Collaboration) “CMS physics: Technical Design Report,” CERN-LHCC-2006-001, CERN-LHCC-2006-028, (2006);
- [48] A. Pukhov, arXiv:hep-ph/0412191;